Plasmon enhancement of Coulomb drag in double-quantum-well systems

Karsten Flensberg
Mikroelektronik Centret, Bygning 345 Øst, Danmarks Tekniske Universitet, DK-2800 Lyngby, Denmark and Dansk Institut for Fundamental Metrologi, Bygning 307, Anker Engelunds Vej 1, DK-2800 Lyngby, Denmark

Ben Yu-Kuang Hu
Mikroelektronik Centret, Bygning 345 Øst, Danmarks Tekniske Universitet, DK-2800 Lyngby, Denmark
(Received 14 July 1995)

We derive an expression for the drag rate (i.e., interlayer momentum transfer rate) for carriers in two coupled two-dimensional gases to lowest nonvanishing order in the screened interlayer electron-electron interaction, valid for *arbitrary* intralayer scattering mechanisms, using the Boltzmann transport equation. We calculate the drag rate for experimentally relevant parameters, and show that for moderately high temperatures ($T \gtrsim 0.2T_F$, where T_F is the Fermi temperature) the dynamical screening of the interlayer results in a large enhancement of the drag rate due to the presence of coupled plasmon modes. This plasmon enhancement causes the scaled drag rate to have a peak (i) as a function of temperature at $T \approx 0.5T_F$, and (ii) as a function of the ratio of densities of the carriers in the two layers when their Fermi velocities are equal. We also show that the drag rate can be significantly affected by the *intralayer* scattering mechanisms; in particular, the drag rate changes approximately by a factor of 2 when the dopant-layer modulation doped structures are moved in from 400 to 100 Å.

I. INTRODUCTION

Coupled quantum wells fabricated by epitaxial growth make up interesting systems for studying electron-electron interactions in low-dimensional systems both experimentally and theoretically. In coupled wells placed within tunneling distance, one can, for instance, study Coulomb gaps in high magnetic fields.[1] For wells separated so that tunneling can be disregarded, the effect of the mutual polarization may become important even at zero magnetic field, and it has been suggested that the interlayer correlations can drive a Wigner crystallization[2] when the coupled plasmon mode goes soft. This is, however, only relevant for low-density systems and has so far not been observed experimentally to our knowledge. At higher densities, coupled collective modes in multilayer systems have been seen in inelastic light scattering experiments.[3,4] In this paper, we discuss another probe of interlayer interactions and the possibility of observing the coupled plasmon modes in bilayer systems, namely, by the so-called Coulomb drag effect,[5,6] where a current in one layer drives a current in the other layer due to the momentum loss caused by interlayer electron-electron scattering events. The Coulomb drag effect has recently attracted much experimental[7–10] and theoretical attention.[11–15]

Normally, the effects of electron-electron collisions only have indirect consequences for transport properties of single isolated quantum wells, because they conserve momentum. The Coulomb drag effect is unique in that it provides an opportunity to directly measure electron-electron interaction through a transport measurement where momentum is transferred from one layer to the other. Since interlayer interactions depend strongly on the many-body effects of the system it is therefore essential to include screening in the theoretical understanding of the measurements.[11–15] Recently, we have pointed out that at intermediate temperatures on the scale of the Fermi temperature the drag effect should in fact be greatly enhanced by "antiscreening" due to coupled plasmon modes.[14]

In this paper, we offer a more detailed study of the predicted plasmon enhancement effect in zero magnetic field. We base our calculation on the random-phase approximation (RPA), which is generally believed to be valid for not too low densities such as, e.g., the experimental realization fabricated by Gramila *et al.*[8] However, for low-density systems such as the electron-hole system studied by Sivan, Solomon, and Shtrikman,[10] the RPA approximation is not able to account for the magnitude of the observed drag effect. This discrepancy between theory and experiment could be an indication of breakdown of RPA due to correlation effects.[15] The Sivan *et al.* system is, however, not relevant for the plasmon enhancement effect studied here due to the large mismatch between the Fermi velocities,[14] as will be explained below.

The results obtained in this paper are based on the Boltzmann equation. Quantum effects neglected by the Boltzmann equation can be shown to be experimentally negligible in the structures we consider.[16,17] We derive a generalized formula for the drag rate that is valid for arbitrary intralayer scattering processes, which reduces to the previously obtained results[8,12,13] for the case of a constant relaxation time approximation.

The role of intralayer carrier-carrier interactions has not been studied so far to our knowledge. As mentioned

above the intralayer interactions usually only have indirect consequences for the transport properties. However, it turns out that the plasmon part of the drag effect is very sensitive to the details of the distribution function. We have solved for the distribution function including intralayer electron-electron interaction using parameters for GaAs-$Al_xGa_{1-x}As$ quantum wells and found that for high-mobility samples where the distance to the δ-doped impurities is fairly large the distrubution is well described by a shifted Fermi-Dirac distribution function and which allows us to assume an energy-independent momentum relaxation rate when calculating the drag rates. This is the situation previously studied by several authors.[8,12–14] However, for the case where the dopant is moved closer to the two-dimensional electron gas the situation is changed and we predict an enhancement of the drag rate because of a larger plasmon contribution in this case. The reason for this enhancement is that the distribution function becomes skewed toward higher energies and the overlap with the plasmon branch consequently becomes larger.

The paper is organized as follows. In Sec. II we discuss the general formula for the drag rate, and in Sec. III we study the RPA approximation of the screening for a coupled two-layer system. The drag rate for the case of shifted Fermi-Dirac distributions, which is applicable when the charged dopants are far from the quantum wells, is studied in Sec. IV. In Sec. V, we study the case when distributions deviate from shifted Fermi-Dirac functions, as when the dopants are close to the quantum wells. Finally, a summary is given in Sec. VI. Technical details are given in a number of appendixes.

II. BOLTZMANN EQUATION CALCULATION OF THE DRAG RATE

In a drag experiment, two doped and independently contacted quantum wells are placed very close to each other.[8] We consider the case typical in experiments where one applies electric field E_1 causing a current of density J_1 to flow in layer one. This sets up an induced electric field E_2 in layer two, where the current is set to zero. (Throughout this paper we denote layer 1 as the driven layer and layer 2 as the dragged layer.) The transresistivity tensor $\rho_{21}^{\beta\alpha}$ is then defined as

$$\sum_{\alpha=x,y} \rho_{21}^{\beta\alpha} J_{1,\alpha} = E_{2,\beta}. \tag{1}$$

By the Onsager relationship, $\rho_{12}^{\alpha\beta} = \rho_{21}^{\beta\alpha}$.

In the case of isotropic parabolic bands, where one has a well-defined effective mass m, one can define a drag rate τ_{21}^{-1} through

$$\rho_{21}^{\alpha\alpha} \equiv \frac{m_1}{n_1 e^2 \tau_{21}}, \tag{2}$$

where n_1 is the carrier density in layer 1. Physically, the drag rate is the net average rate of momentum transferred to each particle in layer 2, per unit drift momentum per particle in layer 1, i.e.,

$$\frac{1}{\tau_{21}} = \frac{\overline{(\partial p_2/\partial t)}}{\overline{p}_1}. \tag{3}$$

where p_i is the momentum per particle in layer i, and the overbar denotes an ensemble average. Note that by this definition, the drag rate is not symmetric; i.e., $\tau_{12}^{-1} = m_2 n_1 m_1^{-1} n_2^{-1} \tau_{21}^{-1}$, which is important when layers 1 and 2 are not identical. We follow the convention of previous authors by denoting τ_{21} as τ_D.

The drag rate has previously been derived using a Boltzmann equation approach[8,12] assuming an *energy-independent* intralayer momentum relaxation time, and also using a memory functional method with a constant relaxation time approximation. This result was recently generalized, using the Kubo formalism, to include energy-dependent impurity scattering rates.[16] Here we shall further generalize this result to *arbitrary* intralayer scattering mechanism within the linear response Boltzmann equation description.

A. Boltzmann equation for coupled quantum wells

We define the function $\psi(\boldsymbol{k})$ that is related to the deviation of the distribution function from equilibrium by

$$\begin{aligned}\delta f(\boldsymbol{k}) \equiv f(\boldsymbol{k}) - f^0(k) &\equiv f^0(k)[1 - f^0(k)]\psi(\boldsymbol{k}) \\ &= -k_B T \left(\frac{\partial f^0(\boldsymbol{k})}{\partial \varepsilon_k}\right) \psi(\boldsymbol{k}),\end{aligned} \tag{4}$$

where $f^0(\boldsymbol{k})$ is the equilibrium Fermi-Dirac distribution function. With this definition, the linearized interlayer electron-electron collision term is[12,18]

$$\begin{aligned}S[\psi_1,\psi_2](\boldsymbol{k}_2) = 2\int \frac{d\boldsymbol{k}_1}{(2\pi)^2}\int \frac{d\boldsymbol{q}}{(2\pi)^2} w(\boldsymbol{q}, \varepsilon_{\boldsymbol{k}_1+\boldsymbol{q}} - \varepsilon_{\boldsymbol{k}_1}) f_1^0(\boldsymbol{k}_1) f_2^0(\boldsymbol{k}_2)[1 - f_1^0(\boldsymbol{k}_1+\boldsymbol{q})][1 - f_2^0(\boldsymbol{k}_2-\boldsymbol{q})] \\ \times [\psi_1(\boldsymbol{k}_1) + \psi_2(\boldsymbol{k}_2) - \psi_1(\boldsymbol{k}_1+\boldsymbol{q}) - \psi_2(\boldsymbol{k}_2-\boldsymbol{q})]\,\delta\left(\varepsilon_{\boldsymbol{k}_1} + \varepsilon_{\boldsymbol{k}_2} - \varepsilon_{\boldsymbol{k}_1+\boldsymbol{q}} - \varepsilon_{\boldsymbol{k}_2-\boldsymbol{q}}\right).\end{aligned} \tag{5}$$

Here $w(q,\omega)$ is the probability of a particle scattering with change of momentum and energy of $\hbar\boldsymbol{q}$ and $\hbar\omega$, respectively. This rate is usually taken to be the Born approximation result $w(q,\omega) = 2\pi\hbar^{-1}|W_{12}(q,\omega)|^2$, where $W_{12}(q,\omega)$ is the dynamically screened interlayer Coulomb interaction matrix element.[19]

We assume that the interlayer interactions are weak, so that these interactions are only kept to lowest order. Then, within linear response to an external driving field E_1, the coupled Boltzmann equations for the system read

$$e_1\boldsymbol{E}_1\cdot\boldsymbol{v}\left(\frac{\partial f_1^0}{\partial\varepsilon}\right) = -\hat{H}_1[\psi_1](\boldsymbol{k}_1), \tag{6a}$$

$$e_2\boldsymbol{E}_2\cdot\boldsymbol{v}\left(\frac{\partial f_2^0}{\partial\varepsilon}\right) = S[\psi_1,\psi_2=0](\boldsymbol{k}_2) - \hat{H}_2[\psi_2](\boldsymbol{k}_2) \tag{6b}$$

where e_i is the carrier charge in layer i and $\hat{H}_i$ is the negative of the linearized *intralayer* collision operator.[18] We have used the assumption of weak interlayer interaction to neglect the interlayer electron-electron collision term in Eq. (6a) and to set $\psi_2(\boldsymbol{k}_2) = 0$ in the interlayer collision term S in Eq. (6b), as these terms are higher order in the interlayer interaction than the other terms in their respective equations. For convenience, hereafter we shall refer to $S[\psi_1,\psi_2=0](\boldsymbol{k}_2)$ simply as $S(\boldsymbol{k}_2)$.

The formal solutions for $\psi_1(\boldsymbol{k}_1)$ and $\psi_2(\boldsymbol{k}_2)$ for $\boldsymbol{E}$ fields in the x direction are

$$\psi_1(\boldsymbol{k}_1) = -e_1E_1\hat{H}_1^{-1}\left[v_{x,1}\left(\frac{\partial f_1^0}{\partial\varepsilon}\right)\right](\boldsymbol{k}_1), \tag{7a}$$

$$\psi_2(\boldsymbol{k}_2) = e_2E_2\hat{H}_2^{-1}\left[v_{x,2}\left(\frac{\partial f_2^0}{\partial\varepsilon}\right)\right](\boldsymbol{k}_2) + \hat{H}_2^{-1}[S](\boldsymbol{k}_2). \tag{7b}$$

We assume the electric field in layer 2 is adjusted so that the current in layer 2 is zero, i.e.,

$$j_{2,x} = -2e_2k_BT\int\frac{d\boldsymbol{k}_2}{(2\pi)^2}v_{2,x}\left(\frac{\partial f_2^0}{\partial\varepsilon}\right)\psi_2(\boldsymbol{k}_2) = 0, \tag{8}$$

which implies, by substitution of Eq. (7b) into Eq. (8),

$$2k_BTe_2^2E_2\int\frac{d\boldsymbol{k}_2}{(2\pi)^2}\,v_{2,x}\left(\frac{\partial f_2^0}{\partial\varepsilon}\right)\hat{H}_2^{-1}\left[v_{2,x}\left(\frac{\partial f_2^0}{\partial\varepsilon}\right)\right](\boldsymbol{k}_2) \equiv n_2e_2\mu_{t,2}E_2$$
$$= -2e_2k_BT\int\frac{d\boldsymbol{k}_2}{(2\pi)^2}v_{x,2}\left(\frac{\partial f_2^0}{\partial\varepsilon}\right)\hat{H}_2^{-1}[S](\boldsymbol{k}_2). \tag{9}$$

The equivalence in Eq. (9) comes from Eq. (A3) in Appendix A, and the $\mu_{t,2}$ is the mobility of layer 2 in the absence of interlayer coupling.

Substituting Eq. (5) [with $\psi_2(\boldsymbol{k}_2) = 0$] into Eq. (9), and using the identities

$$\delta\left(\varepsilon_{\boldsymbol{k}_1} + \varepsilon_{\boldsymbol{k}_2} - \varepsilon_{\boldsymbol{k}_1+\boldsymbol{q}} - \varepsilon_{\boldsymbol{k}_2-\boldsymbol{q}}\right) = \hbar\int_{-\infty}^{\infty}d\omega\;\delta(\varepsilon_{\boldsymbol{k}_1} - \varepsilon_{\boldsymbol{k}_1+\boldsymbol{q}} - \hbar\omega)\delta(\varepsilon_{\boldsymbol{k}_2} - \varepsilon_{\boldsymbol{k}_2-\boldsymbol{q}} + \hbar\omega), \tag{10a}$$

$$f^0(\varepsilon_1)[1-f^0(\varepsilon_2)] = [f^0(\varepsilon_2) - f^0(\varepsilon_1)]n_B(\varepsilon_1-\varepsilon_2), \tag{10b}$$

one obtains

$$n_2e_2\mu_{t,2}E_2 = -4e_2\hbar k_BT\int\frac{d\boldsymbol{q}}{(2\pi)^2}\int_{-\infty}^{\infty}d\omega\;w(\boldsymbol{q},\omega)\,n_B(\hbar\omega)\,n_B(-\hbar\omega)$$
$$\times\left[\int\frac{d\boldsymbol{k}_1}{(2\pi)^2}\,[\psi_1(\boldsymbol{k}_1) - \psi_1(\boldsymbol{k}_1+\boldsymbol{q})][f_1^0(\boldsymbol{k}_1) - f_1^0(\boldsymbol{k}_1+\boldsymbol{q})]\delta(\varepsilon_{\boldsymbol{k}_1} - \varepsilon_{\boldsymbol{k}_1+\boldsymbol{q}} - \hbar\omega)\right]$$
$$\times\left\{\int\frac{d\boldsymbol{k}_2}{(2\pi)^2}\,v_{x,2}\left(\frac{\partial f_2^0}{\partial\varepsilon}\right)\hat{H}_2^{-1}\left[\left\{f_2^0(\boldsymbol{k}_2) - f_2^0(\boldsymbol{k}_2-\boldsymbol{q})\right\}\delta(\varepsilon_{\boldsymbol{k}_2} - \varepsilon_{\boldsymbol{k}_2-\boldsymbol{q}} + \hbar\omega)\right]\right\}. \tag{11}$$

To write Eq. (11) in a more tractable form, we *define* the transport relaxation time of layer i, $\tau_i(\boldsymbol{k}_i)$, for arbitrary intralayer scattering by

$$\psi_i(\boldsymbol{k}_i) = -e\boldsymbol{E}_i\cdot\hat{H}_i^{-1}\left[\boldsymbol{v}_i\left(\frac{\partial f^0}{\partial\varepsilon}\right)\right](\boldsymbol{k}_i) \equiv \frac{e_i\boldsymbol{E}_i\cdot\boldsymbol{v}(\boldsymbol{k}_i)\,\tau_i(\boldsymbol{k}_i)}{k_BT}, \tag{12}$$

in analogy with the case of impurity-dominated scattering (see Appendix A). Then, from Eq. (7a) and the definition in Eq. (12), the term in the large square brackets in Eq. (11) (i.e., involving integration over $\boldsymbol{k}_1$) is equal to

$$\int \frac{d\boldsymbol{k}_1}{(2\pi)^2}\,[\psi_1(\boldsymbol{k}_1)-\psi_1(\boldsymbol{k}_1+\boldsymbol{q})][f_1^0(\boldsymbol{k}_1)-f_1^0(\boldsymbol{k}_1+\boldsymbol{q})]\delta(\varepsilon_{\boldsymbol{k}_1}-\varepsilon_{\boldsymbol{k}_1+\boldsymbol{q}}-\hbar\omega)$$

$$=-\frac{e_1E_1}{k_BT}\int \frac{d\boldsymbol{k}_1}{(2\pi)^2}\,[v_{x,1}(\boldsymbol{k}_1+\boldsymbol{q})\tau_1(\boldsymbol{k}_1+\boldsymbol{q})-v_{x,1}(\boldsymbol{k}_1)\tau_1(\boldsymbol{k}_1)][f_1^0(\boldsymbol{k}_1)-f_1^0(\boldsymbol{k}_1+\boldsymbol{q})]\delta(\varepsilon_{\boldsymbol{k}_1}-\varepsilon_{\boldsymbol{k}_1+\boldsymbol{q}}-\hbar\omega). \tag{13}$$

Note that this quantity is *odd* with respect to ω.[20]

Furthermore, using the fact that $\hat{H}_2^{-1}$ is Hermitian (see Appendix A) and Eq. (12), the term in Eq. (11) in the large curly braces (i.e., involving integration over $\boldsymbol{k}_2$) can be rewritten as

$$\int \frac{d\boldsymbol{k}_2}{(2\pi)^2}\,\left\{f_2^0(\boldsymbol{k}_2)-f_2^0(\boldsymbol{k}_2-\boldsymbol{q})\right\}\delta(\varepsilon_{\boldsymbol{k}_2}-\varepsilon_{\boldsymbol{k}_2-\boldsymbol{q}}+\hbar\omega)\hat{H}_2^{-1}\left[v_{x,2}\left(\frac{\partial f_2^0}{\partial\varepsilon}\right)\right](\boldsymbol{k}_2)$$

$$\begin{aligned}
&=-\frac{1}{k_BT}\int \frac{d\boldsymbol{k}_2}{(2\pi)^2}\,\left\{f_2^0(\boldsymbol{k}_2)-f_2^0(\boldsymbol{k}_2-\boldsymbol{q})\right\}\delta(\varepsilon_{\boldsymbol{k}_2}-\varepsilon_{\boldsymbol{k}_2-\boldsymbol{q}}+\hbar\omega)v_{x,2}(\boldsymbol{k})\tau_2(k)\\
&=\frac{1}{2k_BT}\int \frac{d\boldsymbol{k}_2'}{(2\pi)^2}\,\left\{f_2^0(\boldsymbol{k}_2')-f_2^0(\boldsymbol{k}_2'+\boldsymbol{q})\right\}\Big[\delta(\varepsilon_{\boldsymbol{k}_2'}-\varepsilon_{\boldsymbol{k}_2'+\boldsymbol{q}}-\hbar\omega)v_{x,2}(\boldsymbol{k}_2'+\boldsymbol{q})\tau_2(\boldsymbol{k}_2'+\boldsymbol{q})\\
&\quad+\delta(\varepsilon_{\boldsymbol{k}_2'}-\varepsilon_{\boldsymbol{k}_2'+\boldsymbol{q}}+\hbar\omega)v_{x,2}(\boldsymbol{k}_2')\tau_2(\boldsymbol{k}_2')\Big].
\end{aligned} \tag{14}$$

For the last equality in Eq. (14), we have symmetrized by dividing into two equal parts and performing the variable changes: $\boldsymbol{k}_2=\boldsymbol{k}_2'+\boldsymbol{q}$ in the first term and $\boldsymbol{k}_2=-\boldsymbol{k}_2'$ in the second term and using inversion symmetry in $\boldsymbol{k}$ space. Inserting Eqs. (13) and (14) into Eq. (11), and performing a variable change $\omega\to-\omega$ in the second term in the square brackets of Eq. (14) [which gives an overall minus sign because of the oddness of Eq. (13) with respect to ω] gives the following symmetric form for the transresistivity tensor:

$$\rho_{21}^{\beta\alpha}=\frac{E_2}{n_1e_1\mu_{t,1}E_1}=\frac{\hbar^2}{2\pi e_1e_2n_1n_2k_BT}\int\frac{d\boldsymbol{q}}{(2\pi)^2}\int_0^\infty d\omega\,\frac{|W_{12}(q,\omega)|^2F_1^\alpha(\boldsymbol{q},\omega)]F_2^\beta(\boldsymbol{q},\omega)}{\sinh^2(\hbar\omega/[2k_BT])}. \tag{15}$$

Here, we have used $4n_B(\hbar\omega)n_B(-\hbar\omega)=-\sinh^{-2}(\hbar\omega\beta/2)$ and we have defined the function

$$F^\alpha(\boldsymbol{q},\omega)=\frac{2\pi e}{\hbar\mu_t}\int\frac{d\boldsymbol{k}}{(2\pi)^2}[f^0(\boldsymbol{k})-f^0(\boldsymbol{k}+\boldsymbol{q})]\,\delta(\varepsilon(\boldsymbol{k})-\varepsilon(\boldsymbol{k}+\boldsymbol{q})-\hbar\omega)[v^\alpha(\boldsymbol{k}+\boldsymbol{q})\tau(\boldsymbol{k}+\boldsymbol{q})-v^\alpha(\boldsymbol{k})\tau(\boldsymbol{k})]. \tag{16}$$

As required by the Onsager relation, $\rho_{21}^{\beta\alpha}=\rho_{21}^{\alpha\beta}$ in Eq. (15).

B. Drag rate for isotropic parabolic bands

We concentrate on the case where the bands are isotropic and parabolic, as in the case of the electrons or low-energy holes in GaAs, generally the material of choice so far in performing drag experiments. In this case, when one has a well-defined mass, the mobility can be written in terms of the transport time

$$\mu_t=\frac{e\tau_{\rm tr}}{m}. \tag{17}$$

This transport time is the time that enters the conductivity, $\sigma=ne^2\tau_{\rm tr}/m$. One can write $F^\alpha(\boldsymbol{q},\omega)=q^\alpha Y(q,\omega)$, where

$$\begin{aligned}
Y_i(q,\omega)=\frac{2\pi}{q\tau_{\rm tr,i}}\Big|\int\frac{d\boldsymbol{k}}{(2\pi)^2}\,&\{f_i(\varepsilon(\boldsymbol{k}))-f_i(\varepsilon(\boldsymbol{k}+\boldsymbol{q}))\}\\
\times\;&\{\boldsymbol{k}\tau_i(\varepsilon(\boldsymbol{k}))-(\boldsymbol{k}+\boldsymbol{q})\tau_i(\varepsilon(\boldsymbol{k}+\boldsymbol{q}))\}\\
\times\;&\delta(\varepsilon(\boldsymbol{k})-\varepsilon(\boldsymbol{k}+\boldsymbol{q})-\omega)\Big|.
\end{aligned} \tag{18}$$

Hence, using Eq. (2) and Eq. (15), the drag rate for isotropic parabolic bands can be written as

$$\begin{aligned}
\tau_D^{-1}\equiv\tau_{21}^{-1}=\frac{\hbar^2}{8m_1n_2k_BT\pi^2}&\int_0^\infty dq\;q^3\int_0^\infty d\omega\\
&\times\frac{|W_{12}(q,\omega)|^2Y_1(q,\omega)Y_2(q,\omega)}{\sinh^2(\hbar\omega/[2k_BT])}.
\end{aligned} \tag{19}$$

When $\tau_i(\boldsymbol{k})$ is independent of $\boldsymbol{k}$ the function Y reduces to the usual imaginary part of the polarization function, $\mathrm{Im}[\chi]$, and the drag rate formula in Eq. (19) reduces the result of Refs. 8, 10, and 12. *We emphasize that results*

in Eq. (15) and Eq. (19) hold for arbitrary intralayer scattering mechanism. However, in order to compute the drag rate for a given system one must obtain $\tau(k)$ by first solving for the linear-response distribution function for each layer in the absence of interlayer coupling.

In this paper, we study the drag effect at intermediate temperatures where phonon scattering provides an important contribution to the scattering rates and hence one may expect that the solution of the Boltzmann equation does give a nonconstant $\tau_i(\boldsymbol{k})$. On the other hand, electron-electron interactions tend to pull the distribution function back to a shifted Fermi-Dirac distribution. We have performed a numerical calculation of the distribution function in GaAs-based quantum wells with dopants placed approximately 700 Å away, as in previous experiments (e.g., in Refs. 8 and 10) and found that the distribution functions in these cases can, to a very good approximation, be described by a constant scattering time. Details of the method[21,22] and calculation[22] are given elsewhere. The characteristic time scale for electron-electron scattering is given by[23] $\tau_{e\text{-}e} \approx (h/E_F)\,(E_F/k_BT)^2$. For GaAs doped at 1.5×10^{11} cm^{-2} at 10 K, $\tau_{e\text{-}e} \approx 10^{-11}$ s, as compared to the impurity and phonon scattering times, which are typically of order $\tau_{\mathrm{imp,ph}} \sim 10^{-9}$ s. The relation $\tau_{e\text{-}e} \ll \tau_{\mathrm{imp,ph}}$ explains why the shifted Fermi-Dirac distribution function is a good approximation to the actual solution of the Boltzmann equation.

Therefore, in Sec. IV we shall restrict ourselves to the case where the Y function in Eq. (18) can be replaced by the imaginary part of the polarizability,[8,10,12]

$$\tau_D^{-1} = \frac{\hbar^2}{8m_1n_2k_BT\pi^2}\int_0^\infty dq\; q^3\int_0^\infty d\omega \times\frac{|W_{12}(q,\omega)|^2\mathrm{Im}\chi_1(q,\omega)\mathrm{Im}\chi_2(q,\omega)}{\sinh^2(\hbar\omega/[2k_BT])}. \tag{20}$$

However, we show in Sec. V that in the case when the impurities in the modulation-doped samples are moved in closer to the quantum wells, the momentum relaxation times $\tau(\boldsymbol{k})$ become significantly dependent on $\boldsymbol{k}$, and there are fairly large differences between the drag rates evaluated by Eq. (19) and Eq. (20).

III. COUPLED PLASMON MODES IN THE RANDOM PHASE APPROXIMATION

To calculate the drag rate, one needs to evaluate the dynamically screened Coulomb interaction $W(q,\omega)$, which we do using the RPA. The RPA equations for the coupled two-layer system read[24]

$$\begin{pmatrix} U_{11} \\ U_{21} \end{pmatrix} = \begin{pmatrix} V_{11} \\ V_{21} \end{pmatrix} + \begin{pmatrix} V_{11}\chi_1 & V_{12}\chi_2 \\ V_{21}\chi_1 & V_{22}\chi_2 \end{pmatrix}\begin{pmatrix} U_{11} \\ U_{21} \end{pmatrix}, \tag{21}$$

where the matrix V_{ij} defines the unscreened Coulomb interaction given by $V_{ij} = F_{ij}V(q)$. Here, $V(q) = 2\pi e^2/(\epsilon_0 q) = 2\pi\epsilon_F q_{TF}/(k_F^2 q)$ and F_{ij} are the form factors, for which we use the form for square wells (see, e.g., Ref. 12),

$$F_{ii} = \frac{3x + 8\pi^2/x}{x^2+4\pi^2} - \frac{32\pi^2[1-\exp(-x)]}{x^2(x^2+4\pi^2)^2}, \tag{22a}$$

$$F_{12} = \frac{64\pi^4\sinh^2(x/2)}{x^2(x^2+4\pi^2)^2}e^{-qd}, \tag{22b}$$

where $x = qL$, L is the width of the quantum wells (equal widths are assumed), and d is the center-to-center well separation. The solution for the screened interlayer interaction thus becomes

$$U_{12}(q,\omega) = \frac{V_{12}(q)}{\epsilon(q,\omega)}, \tag{23}$$

where

$$\epsilon(q,\omega) = [1-V_{11}(q)\chi_1(q,\omega)][1-V_{22}(q)\chi_2(q,\omega)] - [V_{12}(q)]^2\chi_1(q,\omega)\chi_2(q,\omega). \tag{24}$$

The collective modes of the coupled electron gas are given by the zeros of the dielectric function. There are two such modes, one where the electron densities in the two layers oscillate in phase, which we call the optic mode, and one where the oscillations are out of phase, referred to as the acoustic mode.[25] At zero temperature $U_{12}(q,\omega)$ has two poles on the real ω axis, giving δ-function peaks. At finite temperatures these poles move off the real ω axis, which implies that they will gain finite widths. In calculating the plasmon dispersions at finite T, we search for the solutions of $\mathrm{Re}[\epsilon(q,\omega(q))] = 0$; so long as the damping is small and the poles are not too far from the real axis, this criterion accurately gives the position of the pole.

While there are simple analytic expressions for $\mathrm{Im}[\chi(q,\omega)]$ and $\mathrm{Re}[\chi(q,\omega)]$ at $T = 0$, none exists at finite temperatures. Since it is necessary to evaluate the χ at finite temperature (using the $T = 0$ expressions for χ does *not* give the required plasmon enhancement, as explained later), we have developed an efficient way of calculating the finite-temperature χ, which is elucidated in Appendix B.

In order to gain insight into the structure of the collective mode dispersions, we take in the following simplifying limit, which allows us to obtain an analytic solution of the dispersion relation of the poles at $T = 0$.

In the case when $qL \ll 1$, one can to a good approximation set $x = qL = 0$ in Eq. (22b) and the form factors reduce simply to $F_{11} = 1$ and $F_{12} = \exp(-qd)$. Then, the dielectric function for two identical layers can be written as

$$\epsilon(q,\omega) = (1-e^{-2qd})[\chi(q,\omega)-\chi_+(q)] \times[\chi(q,\omega)-\chi_-(q)]\{V(q)\}^2, \tag{25}$$

where

$$\chi_\pm(q) = \frac{c_\pm(q)}{V(q)}, \tag{26a}$$

$$c_\pm(q) = \frac{1}{1\pm e^{-qd}}. \tag{26b}$$

From this it is clear that the dispersion of the two col-

lective modes is given by the conditions $\chi(q,\omega_\pm(q)) = \chi_\pm(q)$. The zero-temperature real part of χ is given by[26]

$$V(q)\chi'(q,\omega) = \frac{q_{TF}k_F}{q^2}\left(\frac{q}{k_F} - \sqrt{a_+^2-1} + \sqrt{a_-^2-1}\right), \tag{27}$$

where we have defined $a_\pm = \omega/v_F q \pm q/2k_F$, and used the notation $\chi = \chi' + i\chi''$. We then find for the plasmon solutions

$$\omega_\pm(q) = qv_F\frac{b_\pm\sqrt{1+4/A_\pm}}{2}, \tag{28a}$$

$$b_\pm = c_\pm\frac{q^2}{q_{TF}k_F} + \frac{q}{k_F}, \tag{28b}$$

$$A_\pm = 2c_\pm\frac{q^3}{q_{TF}k_F^2}\left(1 + \frac{qc_\pm}{2q_{TF}}\right). \tag{28c}$$

The small-q behaviors of the plasmon solutions are

$$\omega_+(q) \approx \sqrt{qq_{TF}v_F}, \tag{29a}$$

$$\omega_-(q) \approx qv_F\frac{1+q_{TF}d}{\sqrt{1+2q_{TF}d}} \tag{29b}$$

in agreement with Ref. 27. Thus the optical mode has the familiar square-root behavior while the acoustic mode is linear in q. Because the latter is lower in energy, it gives the dominant contribution to the drag rate at small temperatures, as we show later.

Figure 1 shows the dispersion relation of the plasmons as given by Eq. (28a), for two different values of layer sepation d. Also shown is the part of the q-ω plane where particle-hole excitations are allowed (i.e., $\mathrm{Im}[\chi(q,\omega)] \neq 0$) at zero temperature.

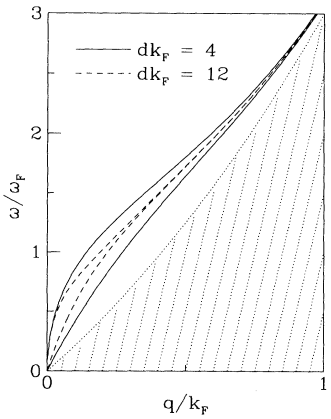

FIG. 1. Plasmon dispersions at zero temperature for two identical wells based on Eq. (28a). The dispersions are shown for two different values of the layer separation $k_Fd = 4$ (solid lines) and $k_Fd = 12$ (dashed lines), and the hatched area is the particle-hole continuum. The lower (upper-) lying branch corresponds to charge-density oscillations in the two layers being out of (in) phase. The modes are well defined only at small q. At larger q, they disappear either by merging together or Landau damping.

In the next section, however, we will see that the plasmon contribution to the drag rate is in fact given by q values in the intermediate range, and thus in order to get a quantitative theory of the collective mode enhancement, use of the small-q expansion is not sufficient, and it is necessary to perform a full numerical calculation.

IV. THE DRAG RATE FOR THE SHIFTED FERMI-DIRAC DISTRIBUTION

As mentioned previously, when the dopants are far enough away from the quantum well ($\gtrsim 400$ Å), the distribution functions are to a very good approximation shifted Fermi-Dirac functions, and one can use Eq. (20) to evaluate τ_D^{-1}. We do so in this section.

A. Plasmon-pole approximation

First, we develop a pole approximation for the plasmon contribition to the drag rate and compare it with the full numerical solution. For frequencies near the zeros of the real part of the dynamical dielectric function we may approximate $\epsilon(q,\omega) \equiv \epsilon' + i\epsilon''$ in Eq. (25) as

$$|\epsilon(q,\omega)| \approx 2V(q)e^{-qd}|\beta_\pm(q)[\omega - \omega_\pm(q)] + i\chi''(q,\omega_\pm)|, \tag{30a}$$

$$\beta_\pm(q) = \left.\frac{d\chi'(q,\omega)}{d\omega}\right|_{\omega=\omega_\pm}. \tag{30b}$$

Inserting the approximate dielectric function into Eq. (20) and assuming that the imaginary part of χ is small, we approximate the Lorenzian by δ functions and obtain

$$\left|\frac{U_{12}(q)}{\epsilon(q,\omega)}\right|^2 \approx \frac{\pi}{4\mathrm{Im}[\chi(q,\omega)]|\beta_\pm(q)|}\delta(\omega - \omega_\pm(q)), \tag{31}$$

which leads to the following two-plasmon contributions to the drag rate:

$$\frac{1}{\tau_\pm} = \frac{\hbar^2}{8\pi e n_2 m_1 kT}\int_0^{q_{c,\pm}} dq\, q^3\frac{\mathrm{Im}[\chi(q,\omega_\pm(q))]}{4|\beta_\pm(q)|\sinh^2[\hbar\omega_\pm(q)\beta/2]}. \tag{32}$$

The parameter q_c in this expression defines the value of q where the plasmon ceases to exist. Operationally, we take $q_{c,\pm}$ to be the wave vector at which the plasmon dispersions disappear (i.e., there are no more solutions $\mathrm{Re}[\epsilon(q,\omega)] = 0$) in the finite-$T$ RPA formalism. Interestingly, the exponential dependence on the well separation d has dropped out of the integrand in Eq. (32). However, $\tau_\pm$ is still d dependent, through the d dependence of $\omega_\pm(q)$, $\beta_\pm(q)$, and q_c. As d is increased, the slope of $\omega_-(q)$ increases and q_c decreases, as evidenced in Fig. 1 (at finite temperatures, the acoustic and optic plasmons merge when they come close, and the merging point gives q_c). Both these effects tend to decrease

the integrand and hence the drag rate. On the contrary, the decrease of $\omega_+(q)$ with increasing d tends to make τ_D^{-1} bigger, but this is generally a weaker effect. Hence, as expected, τ_D^{-1} decreases with increasing well separation. Obtaining a precise analytic functional dependence of τ_D^{-1} on d is difficult, but we have shown numerically that in the plasmon-dominated region $\tau_D^{-1} \sim d^{-\alpha}$ where $\alpha \approx 3$.[14] Also note that Eq. (32) breaks down for large d because in this limit, $\omega_+(q)$ and $\omega_-(q)$ come so close together that the Lorenzians from both these lines overlap. This contradicts the initial assumption that the Lorenzians individually can be approximated by δ functions.

From Eq. (32) we see that the plasmon contribution is given an integral over, among other factors, the imaginary part of χ for frequencies and wave vector corresponding to the plasmon dispersions. Therefore a nonzero $\mathrm{Im}[\chi]$ at $\omega_\pm(q)$, which is outside the $T = 0$ particle-hole continuum, is necessary to obtain any plasmon enhancement effect. Since the $T = 0$ form of $\mathrm{Im}[\chi]$ is always zero at $\omega_\pm(q)$, it will never give a plasmon enhancement. One must therefore use the finite-temperature form of χ in the evaluation of the drag rate.

At small temperatures, $\mathrm{Im}[\chi]$ at $\omega_\pm(q)$ is small because the carriers generally do not have sufficient energy to be excited very far above the Fermi surface. However, at intermediate temperatures (on the scale of the Fermi temperature) there are enough thermally excited particles so that $\mathrm{Im}[\chi]$ at $\omega_\pm(q)$ is large and the plasmons actually dominate the drag response.

In Fig. 2 we show the integrand of the Eq. (20), which gives the drag rate at two different temperatures (for layers of zero width). There are pronounced peaks caused by the presence of plasmons due to the dynamically screened interlayer interaction. We also show the plasmon-pole approximation to the integrand described above, which indicates that this approximation is very good for temperatures less than $0.5T_F$ for the relevant q's which contribute significantly to the integral.

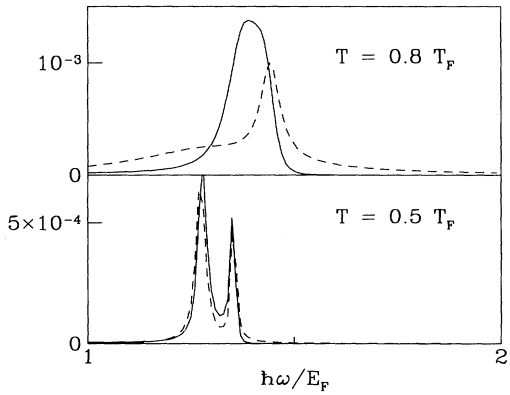

FIG. 2. Scattering rates [integrand of Eq. (20)] as a function of energy transfer $\hbar\omega$, for GaAs coupled quantum wells with equal electron densities of $n = 1.5 \times 10^{11}\,\mathrm{cm}^{-2}$, well separation $d = 8\,k_F^{-1} = 800$ Å, $q = 0.3\,k_F$, and zero well widths, at two different temperatures $T = 0.5T_F$ and $0.8T_F$, where $T_F = 61$ K. The dashed lines are the plasmon-pole approximation to the plasmon peaks, which is used for calculation the pole contributions in Fig. 4. Note how the poles merge and are Landau damped at higher temperatures, implying that the plasmon-pole approximation is not valid for $T \gtrsim 0.6T_F$ and higher.

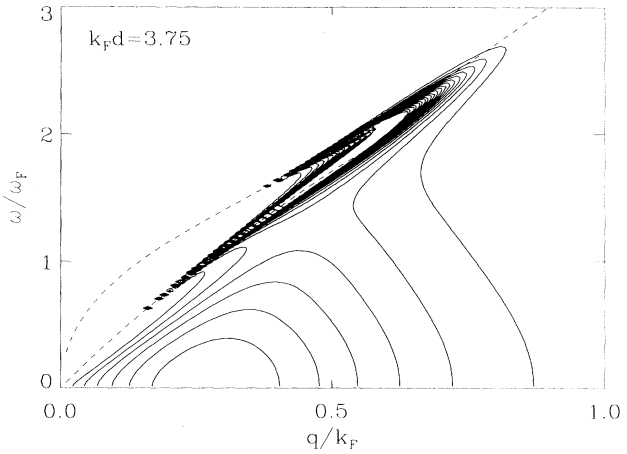

FIG. 3. Contour of the integrand of Eq. (20) for the case of two identical GaAs quantum wells with densities $n = 1.5 \times 10^{11}\,\mathrm{cm}^{-2}$, and a well separation of $d = 3.75\,k_F^{-1} = 375$ Å, well widths of 200 Å, as in the experiment by Gramila *et al.* (Ref. 8), at $T = 18$ K (=0.3 T_F). Adjacent contours differ by $10^{-4}E_F/\hbar = 8 \times 10^8\ \mathrm{s}^{-1}$, and the rightmost contour line equal to $10^{-4}E_F/\hbar$. The dashed lines are the plasmon-pole approximation dispersion curves.

In Fig. 3 we show a contour plot of the integrand of Eq. (20) for $T = 0.3T_F$. Note that the integrand has significant weight at intermediate q and ω values, i.e., up to $q \sim 0.8k_F$ and $\hbar\omega \sim 2E_F$, showing that small ω and q expansions are generally inadequate for calculating τ_D^{-1} at intermediate and high temperatures.

B. Numerical evaluation: τ_D^{-1}

We evaluated τ_D^{-1} for parameters corresponding to high-mobility GaAs samples similar to those of Ref. 8. We did this several different ways. First, we numerically integrated Eq. (20), using the finite-temperature RPA $\mathrm{Im}[\chi]$ obtained through the technique described in Appendix B. Figure 4 shows the result of this full numerical integration of Eq. (20) (solid line). We also solved for the temperature-dependent plasmon poles numerically and used the plasmon-pole approximation described above to obtain the plasmon contribution to the drag rate. One can see that the approximate curves reproduce to a certain degree the enhancement seen in the full solution. At low temperatures the upturn in the drag rate is caused mainly by the acoustic mode, which is lower in energy and hence easier to excite thermally, while at higher temperatures both modes contribute. At even higher temperatures ($T \gtrsim 0.6T_F$) the separation into plasmon and nonplasmon contributions is not well defined because the

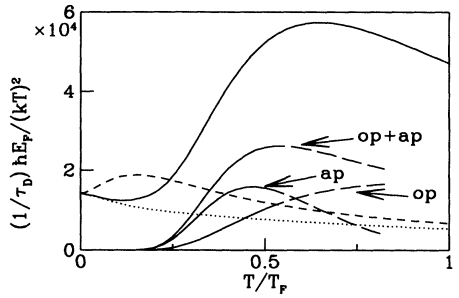

FIG. 4. Temperature dependence of the drag rate scaled by T^2, for the same parameters as in Fig. 3. The full bold curve corresponds to calculations using the finite-T form of $\chi(q,\omega)$, the dotted curve to using the $T = 0$ form of χ (Ref. 13), and the short-dashed curve is based on the static screening approximation (Ref. 12). Also shown are the plasmon-pole approximation estimates for the acoustic plasmon (ap) and optic plasmon (op) contributions to the τ_D^{-1}, and the sum of the two (op+ap). For $T \gtrsim 0.6T_F$, this approximation becomes less reliable due to large Landau damping of the modes, and hence we have plotted the results with dashed lines.

plasmons are heavily Landau damped and merge into the single-particle excitation continuum, cf. Fig. 2. The Landau damping weakens the plasmon enhancement effect, causing the scaled τ_D^{-1} to peak at around $T \approx 0.5T_F$. At extremely high temperatures, $\tau_D^{-1} \sim T^{-3/2}$, as shown in Appendix C.

Figure 4 also shows the result of previously used expressions for the screened interaction. The dashed line represents the approximation where the temperature is set to zero in the polarization function used by Zheng and MacDonald.[13] As discussed earlier, this approximation misses the plasmon contribution, as does the static screened approximation used by Jauho and Smith,[12] given by the dotted curve. Neither of these curves shows the plasmon enhancement demonstrated by the full numerical evaluation of Eq. (20).

We have also evaluated τ_D^{-1} for densities that are smaller and larger than the one used in the experiment of Ref. 8. Calculations relevant for that particular density are shown in Ref. 14. In Fig. 5 we show the scaled drag rate as a function of the temperature. In both plots we have used a well separation of 800 Å. The full curves are for matched densities, while for the dashed (dotted) the density of layer 2 is twice (half) that of layer 1. In Fig. 5(a) the layer 1 density is 5×10^{11} cm^{-2}, and in (b) it is 1×10^{11} cm^{-2}. Since the Fermi temperature is thus 5 times higher in (a), the peak due to the plasmon enhancement occurs at a much higher temperature. Also note that the large peaks in the scaled drag rate occur only in the $n_2/n_1 = 1$ curves.

The insets show the drag rate as a function of the relative density ratio, which show clear peaks at matched densities. The peaks are signatures of the plasmon enhancement effect, and they occur when the Fermi *velocities* $v_{F,i}$ of both subsystems are equal.[14] This is because the size of the plasmon contribution to τ_D^{-1} is determined by the smaller of the $\mathrm{Im}[\chi_i(q,\omega_\pm(q))]$, which is roughly given by the distance between the particle-hole continuum and the plasmon dispersion line on the ω-q plane. The $\min\{\mathrm{Im}[\chi_i]\}$ is maximized at matched $v_{F,i}$. As the $v_{F,i}$'s start to differ from each other, the particle-hole continuum of the subsystem with the smaller v_F, say subsystem 2, starts to move away from the plasmon dispersion lines (which lie above the particle-hole continuum of the subsystem 1 with the larger v_F, 1). Consequently, the $\mathrm{Im}[\chi_2(q,\omega_\pm(q))]$ of the subsystem 2 is decreased with increasing mismatch of v_F, which accordingly decreases the total plasmon contribution to the drag rate. The

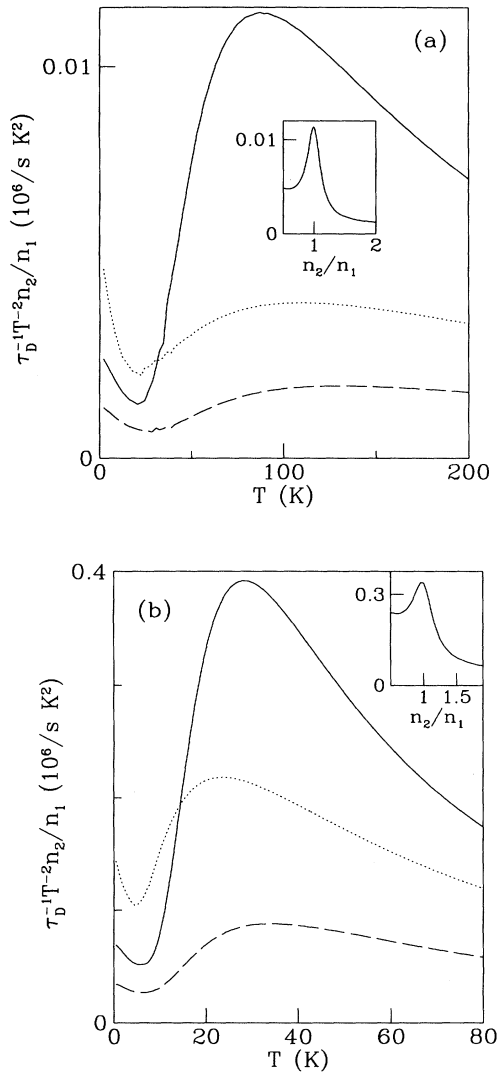

FIG. 5. The drag rate as a function of temperature, for well separation $d = 800$ Å and well width 200 Å, for densities (a) $n_1 = 5 \times 10^{11}$ cm^{-2} and (b) $n_1 = 1 \times 10^{11}$ cm^{-2}. The full, dashed, and dotted lines are for $n_2/n_1 = 1$, 2, and 0.5, respectively. Insets: drag rate as a function of relative density n_2/n_1, when n_1 is fixed and n_2 is allowed to vary at (a) 80 K and (b) 20 K. The peaks at $n_2/n_1 = 1$ are evidence of plasmon enhanced drag.

peak at equal Fermi velocities (and hence matched densities when the masses of the wells are equal) should be the feature of the predicted plasmon enhancement which is easiest to experimentally verify. Other signatures include the aforementioned d^{-3} behavior and the upturn in the temperature scan at approximately $0.2T_F$.[14]

V. DRAG RATE AS A FUNCTION OF DOPANT DISTANCE FROM QUANTUM WELL

Thus far, we have assumed that the $\tau(k)$ is constant (which is equivalent to assuming that the distribution function is a shifted Fermi-Dirac function) and hence Eq. (20) is valid. This is only true if the sum of the impurity and phonon scattering rates is relatively energy independent and/or these rates are much smaller than the intralayer electron-electron scattering rates, as is the case when the dopants are placed approximately 700 Å away from the quantum well. We find, however, that when the impurities are moved closer into the wells, Eq. (20) is no longer valid; in fact, when the impurities are placed 100 Å from the side of the well, it underestimates the drag rate by approximately a factor of 2 when compared to Eq. (19) because it neglects the energy dependence of the momentum relaxation time $\tau(\boldsymbol{k})$.

To evaluate the drag rate in this case, one must be able to calculate the momentum relaxation rate $\tau(\boldsymbol{k})$ in the presence of impurity, phonon, and electron-electron scattering. We adapt the formalism used to study this in three-dimensions[21] to two-dimensions.[22] We assume that the impurities are charged and are in an uncorrelated δ-doped layer a distance s from the side of the quantum well. We calculate $\tau(k)$ including effects of the dynamically screened intralayer electron-electron, screened remote ionized impurity, and screened acoustic (both deformation potential and piezoelectric) phonon[28] scattering. Our calculations indicate that $\tau(k)$ is exceedingly flat when $s = 700$ Å, but as the impurities are moved in $\tau(k)$ starts to show a significant *positive* slope at around $s = 300$ Å. This is because the charged impurity potential is long ranged, implying that it falls off rapidly with increasing momentum transfer,[29] and hence the momentum relaxation time increases with increasing momentum. At large s, the electron-electron scattering, which drives the distribution to a shifted Fermi-Dirac function, suppresses this positive slope. However, as the impurities are moved closer to the well, the impurity scattering and electron-electron scattering rates become comparable, and hence the positive slope in $\tau(k)$ develops.

A positive slope in $\tau(k)$ enhances the drag rate because it implies that there are relatively more carriers at higher energies [see Eq. (12)]. These higher-energy carriers are able to carry more current, which consequently causes increase in the drag rate. The enhancement is even more pronounced when we include dynamical screening because it is the high-energy particles that participate in the plasmon-mediated interlayer Coulomb interaction. In Fig. 6 we show the drag rate as a function of the charged impurities from the side of the wells s (which we assume is the same for both wells), for several different temperatures, all other parameters being fixed. The figure shows that one can obtain an enhancement in the drag rate of approximately a factor of 2 by moving the impurities to within 100 Å of the side of the well, all this coming from the momentum dependence of $\tau(k)$. From the figure, one can see the effect of the plasmons again on τ_D^{-1} in the fact that the enhancement at small s is largest at $T = 30$ K where the plasmon enhancement is the greatest, because a larger number of high-energy particles can now partake in the plasmon-enhanced interlayer scattering.

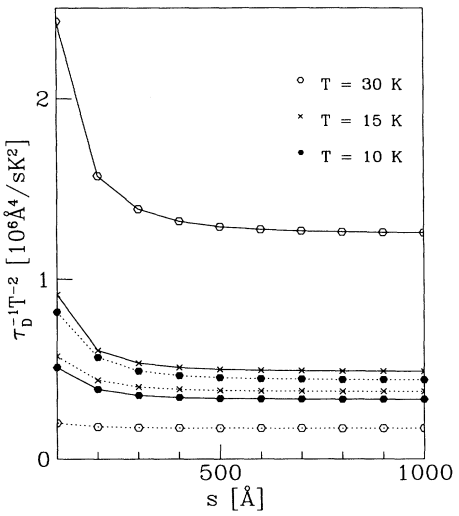

FIG. 6. The drag rate as a function of the distance of the charged dopant layer, s, from the side of the well. The solid (dashed) lines were calculated using full dynamic (static) screening, and $T = 15$, 20, and 30 K. The parameters used were $n = 1.5 \times 10^{11}$ cm^{-2}, $d = 375$ Å, and well width of 100 Å in GaAs. For $s \gtrsim 400$ Å, the distribution functions are very close to shifted Fermi-Dirac functions. As s decreases, the distribution functions deviate from shifted Fermi-Dirac functions, and the drag rate increases markedly.

Finally, since we have studied the drag rate in the case where the absolute magnitude of the impurity scattering rate is large (because s is small) one could ask if the diffusive form of the polarizability function[13,16,17] at small q and ω has any effect on our calculations at experimentally relevant temperatures. We conclude it does not because the crossover temperature below which the diffusive effect should be seen goes as[13] $\sim 0.1\text{K}\exp[-0.9(\ell/d)^2]$. Since d is on the order of 400 Å, and ℓ, the mean free path, is approximately 0.1 to 1 μm for $s = 100$ Å, the crossover temperature is extremely small and experimentally irrelevant.

VI. DISCUSSION AND SUMMARY

Using the Boltzmann equation, we have derived a formula for the transresistivity of coupled two-dimensional electron gases, valid for arbitrary intralayer scattering, to lowest nonvanishing order in the interlayer interaction.

While the Boltzmann equation does not include quantum effects such as weak localization, it has been shown[17,16] that these effects for systems where $k_F\ell \gg 1$ are negligible. The transresistivity depends on the momentum relaxation times $\tau_i(\boldsymbol{k})$ of both layers, which are given by the linear-response solution of the distribution function to an applied electric field.

For isotropic parabolic bands, one can define a drag rate that is proportional to the transresistivity. In this case, in the limit where $\tau(k)$ is a constant, one regains the previously obtained result, Eq. (20), from our result, Eq. (19). A constant $\tau(k)$ is equivalent to a shifted Fermi-Dirac distribution function under application of a small electric field. In experiments done previously, where the dopant layer in the modulation-doped structures is relatively far away from the quantum wells, $\tau(k)$ is in fact relatively constant over the relevant energy range (i.e., within a few k_BT from the chemical potential), because the electron-electron scattering rate, which tends to drive the distribution to a shifted Fermi-Dirac function, dominates over all other scattering rates. Thus, for calculations involving these structures, we have used Eq. (20).

The interlayer coupling is given by the screened Coulomb interaction. Due to the presence of plasmons, both acoustic and optic, the interaction can be significantly enhanced, as these plasmons serve to "antiscreen" the interaction. At low temperatures, the plasmons are "frozen out," and hence they play no role. At higher temperatures, however, the plasmons can enhance the drag rate by almost an order of magnitude over interactions that exclude dynamic effects of the coupled electron gas system. We have shown that the maximum plasmon enhancement occurs around 30 K for GaAs when both wells are doped at 1.5×10^{11} cm^{-2}. Furthermore, because the plasmon enhancement is most effective when the Fermi velocities of the two electron gases are equal, one should see a peak in the τ_D^{-1} as the ratio of densities of the electron gases n_2/n_1 is varied through 1.

We have also investigated the effect of moving impurities closer to the quantum wells, which gives $\tau(k)$ a positive slope. This increases the number of high-energy (and hence large current carrying) particles and hence also enhances the drag rate. The effect is largest when the plasmon effect is the greatest. One obtains an enhancement of approximately a factor of 2 when impurities are moved in from $s = 400$ Å to $s = 100$ Å.

ACKNOWLEDGMENTS

We thank A.-P. Jauho for numerous discussions. K.F. was supported by the Carlsberg Foundation.

APPENDIX A: BOLTZMAN EQUATION FOR SINGLE LAYER

In this appendix, we describe the formalism for the Boltzmann equation in a single quantum well, which we use in the main text.

1. Formalism for intralayer scattering

The linearized form of the Boltzmann equation for (positively charged) carriers with an electric field $\boldsymbol{E}$ is

$$e\boldsymbol{E}\cdot\left(\frac{\partial f^0}{\partial \boldsymbol{p}}\right) \equiv e\boldsymbol{E}\cdot\boldsymbol{v}\left(\frac{\partial f^0}{\partial \varepsilon}\right) = -\hat{H}[\psi(\boldsymbol{k})]. \tag{A1}$$

From the principle of detailed balance, one can show that $\hat{H}$ is a Hermitian operator,[18] i.e., for arbitrary functions $a(\boldsymbol{k})$ and $b(\boldsymbol{k})$,

$$\int d\boldsymbol{k}\, a(\boldsymbol{k})\, \hat{H}[b](\boldsymbol{k}) = \int d\boldsymbol{k}\, b(\boldsymbol{k})\, \hat{H}[a](\boldsymbol{k}). \tag{A2}$$

Therefore, the current in the β direction is given by Eqs. (4) and (A1),

$$\begin{aligned} j_\beta &= 2e\int \frac{d\boldsymbol{k}}{(2\pi)^d}\, v_\beta\, \delta f(\boldsymbol{k}) \\ &= -2ek_BT\int \frac{d\boldsymbol{k}}{(2\pi)^d}\, v_\beta(\boldsymbol{k})\left(\frac{\partial f^0}{\partial \varepsilon}\right)\psi(\boldsymbol{k}) \\ &= 2k_BTe^2\sum_\alpha E_\alpha \int \frac{d\boldsymbol{k}}{(2\pi)^d}\, v_\beta(\boldsymbol{k})\left(\frac{\partial f^0}{\partial \varepsilon}\right)(\boldsymbol{k})\, \hat{H}^{-1}\left[v_\alpha\left(\frac{\partial f^0}{\partial \varepsilon}\right)\right](\boldsymbol{k}) \\ &\equiv ne\sum_\alpha \mu_t^{\beta\alpha}E_\alpha, \end{aligned} \tag{A3}$$

where the factor of 2 is for spin, and $\mu_t^{\beta\alpha}$ is mobility tensor of the system.

2. Impurity scattering

We now examine a concrete example, an isotropic system dominated by impurity scattering, in which case the linearized collision operator is given by

$$-\hat{H}[\psi](\boldsymbol{k}) = k_BT\left(\frac{\partial f^0}{\partial \varepsilon}\right)(k)\,\tau^{-1}(k)\,\psi(\boldsymbol{k}), \tag{A4}$$

where $\tau(k)$ is the *transport* lifetime.[18] The inverse of $\hat{H}$ is trivial,

$$\hat{H}^{-1}[g](\boldsymbol{k}) = -\frac{g(\boldsymbol{k})\tau(\boldsymbol{k})}{k_B T\,(\partial f^0/\partial\varepsilon)(\boldsymbol{k})}, \tag{A5}$$

and hence the solution of Eq. (A1), for $\boldsymbol{E}$ in the x direction, is

$$\psi(\boldsymbol{k}) = \frac{eE\,v_x(\boldsymbol{k})\,\tau(k)}{k_B T}. \tag{A6}$$

APPENDIX B: NUMERICAL EVALUATION OF THE FINITE TEMPERATURE POLARIZATION FUNCTION

Here we describe an efficient technique for calculating the finite-temperature 2D-RPA χ for an isotropic parabolic band. The RPA χ is given by

$$\chi(\boldsymbol{q},\omega) = \frac{2m}{\hbar^2}\int \frac{d\boldsymbol{k}}{(2\pi)^2}\frac{f^0(\boldsymbol{k}+\boldsymbol{q}/2) - f^0(\boldsymbol{k}-\boldsymbol{q}/2)}{\boldsymbol{k}\cdot\boldsymbol{q} - m\omega/\hbar - i0^+}, \tag{B1}$$

where f^0 is the Fermi distribution. We define the following nondimensional quantities

$$Q = q/k_F,\quad K = k/k_F,\quad \Omega = \hbar\omega/E_F,$$

$$t = k_B T/E_F,\quad \tilde{\mu} = \mu/E_F,\quad \tilde{\chi} = \frac{\chi}{m/(\pi\hbar^2)}, \tag{B2}$$

where $k_F = (2\pi n)^{1/2}$ (n is the density), and $E_F = \hbar^2 k_F^2/(2m)$. Note that $\tilde{\chi}$ is normalized by the value of $\chi(q\to 0,\omega = 0; T = 0)$. In these units,

$$\tilde{\chi}(Q,\Omega) = \frac{1}{2\pi}\int dK_x\,dK_y\,\frac{f^0(K_x + Q/2, K_y) - f^0(K_x - Q/2, K_y)}{K_x Q - \Omega/2 - i0^+}, \tag{B3}$$

where

$$f^0(K_x,K_y) = \frac{1}{\exp([K_x^2 + K_y^2 - \tilde{\mu}]/t) + 1},\quad \tilde{\mu} = t\,\ln(e^{1/t} - 1). \tag{B4}$$

1. Imaginary part of χ

The imaginary part of χ is given by

$$\begin{aligned}\mathrm{Im}[\tilde{\chi}(Q,\Omega)] &= \frac{1}{2Q}\int_{-\infty}^{\infty} dK_y\, f^0\left(\frac{\Omega}{2Q} + \frac{Q}{2}, K_y\right) - f^0\left(\frac{\Omega}{2Q} - \frac{Q}{2}, K_y\right)\\ &= \frac{\sqrt{t\pi}}{2Q}\left[\mathcal{F}_{-1/2}\left(\frac{A_+}{t}\right) - \mathcal{F}_{-1/2}\left(\frac{A_-}{t}\right)\right],\quad A_\pm = \tilde{\mu} - \left(\frac{\Omega}{2Q} \pm \frac{Q}{2}\right)^2,\end{aligned} \tag{B5}$$

where

$$\mathcal{F}_{-1/2}(x) = \frac{1}{\sqrt{\pi}}\int_0^\infty dy\,\frac{y^{-1/2}}{\exp(y-x)+1} \tag{B6}$$

is the Fermi function of order $-1/2$.[30] $\mathcal{F}_{-1/2}$ is a well-known function, and many excellent approximation schemes are available to evaluate it.[31]

2. Real part of χ

We use the expression by Maldague[32]

$$\chi(q,\omega;\mu,T) = \int_0^\infty d\mu'\,\chi(q,\omega;\mu',T=0)\frac{1}{4k_B T\cosh^2[(\mu-\mu')/(2k_B T)]}. \tag{B7}$$

Letting $a_\pm = \frac{1}{2}(\frac{\Omega}{Q} \pm Q)$ and using the known form for $\chi(q,\omega;T=0)$, we obtain

$$\mathrm{Re}[\tilde{\chi}(Q,\Omega)] = -\int_0^\infty d\tilde{\mu}' \frac{1}{4t\cosh^2[(\tilde{\mu}-\tilde{\mu}')/(2t)]}\Big[1 - \frac{\mathrm{sgn}(a_+)}{Q}\sqrt{a_+^2-\tilde{\mu}'}\,\theta(a_+^2-\tilde{\mu}') + \frac{\mathrm{sgn}(a_-)}{Q}\sqrt{a_-^2-\tilde{\mu}'}\,\theta(a_-^2-\tilde{\mu}')\Big]$$
$$= -\frac{1}{\exp(-\tilde{\mu}/t)+1} + \frac{\mathrm{sgn}(a_+)}{Q}M_t(a_+^2) - \frac{\mathrm{sgn}(a_-)}{Q}M_t(a_-^2), \tag{B8}$$

where

$$M_t(x) = \int_0^x d\tilde{\mu}' \frac{1}{4t\cosh^2\left([\tilde{\mu}'-\tilde{\mu}(t)]/(2t)\right)}(x-\mu')^{1/2}. \tag{B9}$$

For any given temperature, this function $M_t(x)$ need only be evaluated once, and then a polynomial, Padé, or a spline fit can be made to it. Then, $\mathrm{Re}[\chi(q,\omega)]$ can be evaluated with this fitted function, using Eq. (B8). Caution, however, should be exercised when $Q \ll 1$ and Ω/Q is not small. Then, the terms $\pm Q^{-1}M_t(a_\pm)$ in Eq. (B8) are large and approximately cancel, leading to large numerical uncertainly. We got around this problem by using the well-known asymptotic form $\mathrm{Re}[\tilde{\chi}(Q,\Omega)] = 2Q^2/\Omega^2$, which can be derived from Eq. (B8). This form should be used in the regions when numerical inaccuracies plague the form given in Eq. (B8).

Note that this technique for calculating the RPA-χ is not restricted to equilibrium situations. For a nonequilibrium isotropic distribution function $f(k)$, one need only replace f^0 in Eq. (B5) and $1/4k_BT\cosh^2[(\mu-\mu')/(2k_BT)]$ in Eq. (B7) by f and $\partial f/\partial\varepsilon$, respectively.

APPENDIX C: THE LARGE TEMPERATURE LIMIT $T \gg T_F$

In the case of very large temperature, the Coulomb interactions are basically unscreened because the typical wave-vector transfers are much larger than the Debye screening wave number, $q_D = 2\pi e^2 n/(\epsilon_0 k_B T)$, and one can assume that the interlayer interaction is the bare unscreened interaction. Then, under further assumptions that the carriers are nondegenerate and the intralayer momentum scattering rate is constant, we show that the drag rate goes as $\tau_D^{-1} \propto T^{-3/2}$. Since $\tau_D^{-1} \propto T^2$ for small T, the drag rate must peak at some temperature.

The polarization function for a Maxwell-Boltzmann distribution in the RPA is

$$\tilde{\chi}(\tilde{q},\tilde{\omega}) = \frac{1}{2t\tilde{q}}\left[Z\left(\frac{\tilde{\omega}}{2\tilde{q}}+\frac{\tilde{q}}{2}\right) - Z\left(\frac{\tilde{\omega}}{2\tilde{q}}-\frac{\tilde{q}}{2}\right)\right], \tag{C1}$$

where Z is the plasma dispersion function.[33] Here as before, $\tilde{\chi} = \chi/[m/(\hbar^2\pi)]$ and $t = T/E_F$, whereas the other variables with tildes are defined as being normalized with respect to temperature,

$$\tilde{q} = \hbar q/\sqrt{2mk_BT},$$
$$\tilde{\omega} = \frac{\hbar\omega}{k_BT},$$
$$\tilde{d} = d\sqrt{2mk_BT}\hbar^{-1}. \tag{C2}$$

The classical limit ($\tilde{q} \ll 1$) of the polarization function χ_{cl} [which is valid here because the $\tilde{q}$ integration is cut off at small $\tilde{q}$; see below] only depends on the ratio $\tilde{\omega}/\tilde{q}$,

$$\tilde{\chi}_{\mathrm{cl}}(\tilde{\omega}/\tilde{q}) = \frac{1}{2t}Z'\left(\frac{\tilde{\omega}}{2\tilde{q}}\right). \tag{C3}$$

The imaginary part is given by[33]

$$\mathrm{Im}[\chi_{\mathrm{cl}}(\tilde{\omega}/\tilde{q})] = -\frac{\tilde{\omega}\sqrt{\pi}}{2t\tilde{q}}\exp\left(-\frac{\tilde{\omega}^2}{4\tilde{q}^2}\right). \tag{C4}$$

From Eq. (20), the drag rate for identical layers is

$$\tau_D^{-1} = \left\{\frac{\hbar q_F^4}{8\pi^2 nm}\left(\frac{2\pi e^2 m}{\epsilon_0\pi\hbar^2 q_F}\right)^2\right\} t\int_0^\infty d\tilde{q}\,\tilde{q}^3 \times \int_0^\infty d\tilde{\omega}\,\frac{\exp(-2\tilde{q}\tilde{d})}{\tilde{q}^2\sinh^2(\tilde{\omega}/2)}\,\frac{\pi\tilde{\omega}^2}{4t^2\tilde{q}^2}\exp\left(-\frac{\tilde{\omega}^2}{2\tilde{q}^2}\right). \tag{C5}$$

Having nonidentical layers simply leads to a change in the prefactor. Defining $\tilde{\tau}_D^{-1}$ as τ_D^{-1} divided by the non-temperature-dependent prefactor in the curly braces in the above equation yields

$$\tilde{\tau}_D^{-1} = \frac{\pi}{4t}\int_0^\infty d\tilde{q}\,\tilde{q}^{-1}\exp(-2\tilde{q}\tilde{d}) \times \int_0^\infty d\tilde{\omega}\frac{\tilde{\omega}^2\exp[-\tilde{\omega}^2/(2\tilde{q}^2)]}{\sinh^2(\tilde{\omega}^2/2)}. \tag{C6}$$

Since $\tilde{d} \propto T^{1/2}$, for large T the integrals are cut off at small $\tilde{q}$. The presence of the Gaussian term in the $\tilde{\omega}$ integral implies that this integral is also cut off at small values, and hence an expansion $\sinh^2(\tilde{\omega}/2) \approx \tilde{\omega}^2/4$ can be made. This gives

$$\tilde{\tau}_D^{-1} \approx \pi t^{-1}\int_0^\infty d\tilde{q}\,\tilde{q}^{-1}\int_0^\infty d\tilde{\omega}\,\exp[-\tilde{\omega}^2/(2\tilde{q}^2)],$$
$$= \frac{\pi}{t}\sqrt{\frac{\pi}{2}}\int_0^\infty d\tilde{q}\,\exp(-2\tilde{q}\tilde{d}),$$
$$= \left(\frac{\pi}{2}\right)^{3/2}\frac{1}{t\tilde{d}}. \tag{C7}$$

Since $t \propto T$ and $\tilde{d} \propto T^{1/2}$, this shows that the temperature dependence of the drag rate in the large-temperature

limit, given an energy-independent intralayer momentum relaxation rate, is

$$\tau_D^{-1} \propto T^{-3/2}. \tag{C8}$$

In actual fact, this asymptotic behavior is reached very slowly. Our numerical evaluation of the drag rate indicates that for the experimental parameters of Ref. 8, this behavior of τ_D^{-1} occurs only when $T \gg 10T_F$, and hence is not experimentally observable for these parameters.

[1] J. P. Eisenstein, G. S. Boebinger, L. N. Pfeiffer, K. W. West, and Song He, Phys. Rev. Lett. **68**, 1383 (1992).

[2] L. Świerkowski and D. Neilson, Phys. Rev. Lett. **67**, 240 (1991).

[3] A. Pinczuk, M. G. Lamont, and A. C. Gossard, Phys. Rev. Lett. **56**, 2092 (1986).

[4] G. Fasol *et al.*, Phys. Rev. Lett. **56**, 2517 (1986).

[5] M. B. Pogrebinskii, Fiz. Tekh. Poluprovodn. **11**, 637 (1977) [Sov. Phys. Semicond. **11**, 372 (1977)].

[6] P. J. Price, Physica (Amsterdam) **117B**, 750 (1983).

[7] P. M. Solomon, P. J. Price, D. J. Frank, and D. C. L. Tulipe, Phys. Rev. Lett. **63**, 2508 (1989).

[8] T. J. Gramila *et al.*, Phys. Rev. Lett. **66**, 1216 (1991).

[9] T. J. Gramila, J. P. Eisenstein, A. H MacDonald, L. N. Pfeiffer, and K. W. West, Phys. Rev. B **47**, 12 957 (1993); Physica (Amsterdam) **197B**, 442 (1994).

[10] U. Sivan, P. M. Solomon, and H. Shtrikman, Phys. Rev. Lett. **68**, 1196 (1992).

[11] B. Laikhtman and P. M. Solomon, Phys. Rev. B **41**, 9921 (1990); I. I. Boiko and Yu. M. Sirenko, Phys. Status Solidi **159**, 805 (1990); P. M. Solomon and B. Laikhtman, Superlatt. Microstruct. **10**, 89 (1991); A. G. Rojo and G. D. Mahan, Phys. Rev. Lett. **68**, 2074 (1992); H. C. Tso, P. Vasilopoulos, and F. M. Peeters, *ibid.* **68**, 2516 (1992); **70**, 2146 (1993); H. C. Tso and P. Vasilopoulos, Phys. Rev. B **45**, 1333 (1992); D. I. Maslov, *ibid.* **45**, 1911 (1992); J.-M. Duan and S. Yip, Phys. Rev. Lett. **70**, 3647 (1993); H. L. Cui, X. L. Lei, and N. J. M. Horing, Superlatt. Microstruct. **13**, 221 (1993); E. Shimshoni and S. L. Sondhi, Phys. Rev. B **49**, 11 484 (1994).

[12] A.-P. Jauho and H. Smith, Phys. Rev. B **47**, 4420 (1993).

[13] L. Zheng and A. H. MacDonald, Phys. Rev. B **48**, 8203 (1993).

[14] K. Flensberg and B. Y.-K. Hu, Phys. Rev. Lett. **73**, 3572 (1994).

[15] L. Świerkowski, J. Szymański, and Z. W. Gortel, Phys. Rev. Lett. **74**, 3245 (1995).

[16] K. Flensberg, B. Y.-K. Hu, A.-P. Jauho, and J. Kinaret, Phys. Rev. B **52**, 14 761 (1995).

[17] A. Kamenev and Y. Oreg, Phys. Rev. B **52**, 7516 (1995).

[18] H. Smith and H. H. Jensen, *Transport Phenomena* (Clarendon Press, Oxford, 1989).

[19] We have assumed that the scattering rate only depends on the momentum and energy transfered. This is valid when the unit-cell periodic part of the Bloch wave function of the electron does not vary significantly over the region of the Broullioun zone relevant to the problem (see, e.g., Ref. 29, Chap. 3). When this is not true, e.g., in the case of holes in the warped region of the Brillouin zone of GaAs, the expression for τ_D cannot be deconvolved in the manner described further on in this paper, and the calculation of τ_D generally requires the numerical evaluation of a six-dimensional integral.

[20] This can be shown by interchanging changing variables $\boldsymbol{k}_1' = -\boldsymbol{k}_1 - \boldsymbol{q}$, and using inversion symmetry in $\boldsymbol{k}$ space. Note that inversion symmetry in $\boldsymbol{k}$ space does *not* require inversion symmetry in real space, but merely time-reversal symmetry of the unperturbed system.

[21] B. A. Sanborn, Phys. Rev. B **51**, 14 256 (1995).

[22] B. Y.-K. Hu and K. Flensberg (unpublished).

[23] C. Hodges, H. Smith, and J. W. Wilkins, Phys. Rev. B **4**, 302 (1971); G. F. Giuliani and J. J. Quinn, *ibid.* **26**, 4421 (1982).

[24] See, e.g., Ben Yu-Kuang Hu and S. Das Sarma, Phys. Rev. B **48**, 5469 (1993), Appendix A.

[25] S. D. Sarma and A. Madhukar, Phys. Rev. B **23**, 805 (1981).

[26] F. Stern, Phys. Rev. Lett. **18**, 546 (1967).

[27] G. E. Santoro and G. F. Guiliani, Phys. Rev. B **37**, 937 (1988).

[28] T. Kawamura and S. D. Sarma, Phys. Rev. B **45**, 3612 (1992).

[29] B. K. Ridley, *Quantum Processes in Semiconductors*, 2nd. ed. (Oxford Univ. Press, Oxford, 1988).

[30] J. S. Blakemore, *Semiconductor Statitics* (Pergamon, New York, 1962; reprinted by Dover, New York, 1987).

[31] W. J. Cody and Henry C. Thatcher, Jr., Math. Comput. **21**, 30 (1967). Note, however, that their coefficients for the approximate function for $x \geq 4$ give inaccurate results. We have generated a better approximation simply using well-known Padé fitting schemes [see, e.g., William H. Press, Saul A. Teukolsky, William T. Vetterling, and Brian P. Flannery, *Numerical Recipes*, 2nd. ed. (Cambridge Univ. Press, Cambridge, 1992)].

[32] P. F. Maldague, Surf. Sci. **73**, 296 (1978).

[33] B. D. Fried and S. D. Conte, *The Plasma Dispersion Function* (Academic, New York, 1961).